JOURNAL OF SPACECRAFT AND ROCKETS
Vol. 42, No. 1, January–February 2005

Analysis of Magnetoplasmadynamic Interaction in the Boundary Layer of a Hypersonic Wedge

Carlo A. Borghi,* Mario R. Carraro,† and Andrea Cristofolini‡
University of Bologna, I-40135 Bologna, Italy

A model for the analysis of the magnetoplasmadynamic regime, devoted to magnetohydrodynamic (MHD) systems in a hypersonic flight, is presented. In the assumption of a low-magnetic-Reynolds-number regime, the model couples a time-dependent formulation of fluid dynamics with steady-state electrodynamics. The Navier–Stokes equations are discretized by means of a finite volume formulation. The electrodynamics is discretized by means of a finite element method. The model has been utilized for the analysis of the MHD interaction in the boundary layer of a test body in a wind tunnel. The activity is aimed to design the experimental activity in the frame of an Italian Space Agency research project on the MHD interaction in hypersonic flows. Calculations have shown that MHD interaction can be greatly weakened by the effect of the Hall current.

Nomenclature

$\boldsymbol{B}$	=	magnetic flux density
$\boldsymbol{D}$	=	electric displacement
$\boldsymbol{E}$	=	electric field
e_i	=	specific internal energy
$\boldsymbol{H}$	=	magnetic field strength
$\boldsymbol{J}$	=	electric current density
K	=	thermal conductivity
L_c	=	characteristic length
m_e	=	electron mass
n_e	=	electron density
p	=	pressure
T	=	temperature
$\boldsymbol{u}$	=	velocity
β_e	=	electron Hall parameter
μ_e	=	electron mobility
ν_{eH}	=	collision frequency between electron and heavy particle
ρ	=	mass density
σ	=	scalar electrical conductivity
$\boldsymbol{\tau}$	=	stress tensor
φ	=	electric scalar potential
ω_p	=	plasma frequency

Introduction

THE concept of hypersonic flight has recently received an increasing interest. Hypersonic flight has been usually linked to the reentering of space vehicles into the atmosphere. A new wide range of applications of hypersonic flight is related to the development of a single-stage-to-orbit (SSTO) vehicle, which is now one of the main prerequisites for the commercial exploitation of space flight. An SSTO vehicle should be powered by airbreathing engines: a turbojet for low-speed operations, such as takeoff and landing: a ramjet for vehicle Mach numbers between 4 and 7; and finally a scramjet that could accelerate the vehicle up to Mach 20 in the upper layers of the Earth's atmosphere. Many applications of magnetohydrodynamic (MHD) interaction in hypersonic vehicles have been proposed and discussed.[1] An MHD system has been proposed to control the fluid dynamics at the inlet of the scramjet; in the Russian AJAX project, MHD techniques are utilized to bypass kinetic energy of the working fluid from the supersonic diffuser to the nozzle, reducing the flow velocity in the combustion chamber to an acceptable value even for high vehicle Mach numbers. Another interesting opportunity is to control boundary-layer phenomena, shock waves, and heat fluxes by means of MHD interaction.

Ionization methods vary according to the hypersonic regime. For moderate Mach numbers ($M < 7$), a suitable ionization degree can be reached by injecting in the gas an alkaline element, K or Cs, with a low ionization potential. For the intermediate regime ($7 < M < 12$), a strong MHD interaction can be obtained by applying rf or electron beams to excite the gas molecules. For highly hypersonic regimes ($M > 12$), a suitable degree of ionization is obtained solely by relying on the fluid dynamic conditions.

In Fig. 1 the basic concept of the MHD interaction for the flow control regime in the boundary layer of a hypersonic vehicle is shown. The current I flowing in the conductor located under the leading edge of the body generates a magnetic flux density which, interacting with the gas flowing with velocity $\boldsymbol{u}$, produces a force per electric charge unit $\boldsymbol{u} \times \boldsymbol{B}$. If the gas presents some ionization degree, the electromotive force generates a current density $\boldsymbol{J}$ which, interacting with the magnetic flux density, originates a body force $\boldsymbol{J} \times \boldsymbol{B}$ on the gas, opposite to the flow direction.

In this paper, a two-dimensional time-dependent numerical model is utilized for the preliminary calculation of the magnetoplasmadynamic regime around a wedge. The aim of the analysis is to get an insight into the effect of the electrical configuration of the wedge on the MHD interaction. The result obtained will constitute essential knowledge for the design and the optimization of the experimental activities to be performed in the frame of the Italian Space Agency research project "MHD Interaction in Hypersonic flows."

Physical Model

The fluid dynamic equations are given by the continuity equation for mass, momentum, and energy, and by the state equations of gas as follows:

$$\frac{\partial \boldsymbol{U}}{\partial t} + \nabla \cdot \boldsymbol{F} = \boldsymbol{Q} \tag{1}$$

$$p = p(\rho, T), \qquad e_i = e_i(\rho, T) \tag{2}$$

Presented as Paper 2003-3761 at the AIAA 34th Plasmadynamics and Lasers Conference, Orlando, FL, 23–26 June 2003; received 22 July 2003; revision received 26 January 2004; accepted for publication 28 January 2004.

*Full Professor, Department of Electrical Engineering, Viale Risorgimento, 2; ca.borghi@mail.ing.unibo.it. Member AIAA.

†Ph.D. Student, Department of Electrical Engineering, Viale Risorgimento, 2; mario.carraro@mail.ing.unibo.it.

‡Professor, Department of Electrical Engineering, Viale Risorgimento, 2; andrea.cristofolini@mail.ing.unibo.it.

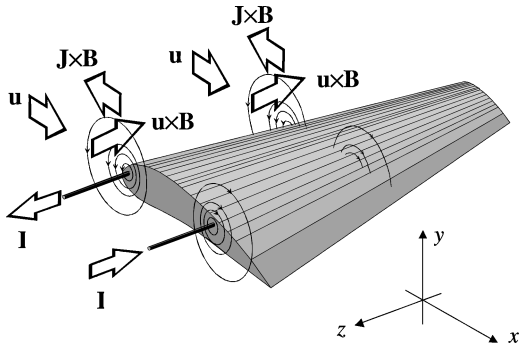

Fig. 1 Schematic of the problem.

where the quantities $\boldsymbol{U}$, $\boldsymbol{F}$, and $\boldsymbol{Q}$ are defined as

$$\boldsymbol{U} = \begin{vmatrix} \rho \\ \rho\boldsymbol{u} \\ e_i \end{vmatrix}, \qquad \boldsymbol{F} = \begin{vmatrix} \rho\boldsymbol{u} \\ \rho\boldsymbol{u}\boldsymbol{u} + p\boldsymbol{I} - \boldsymbol{\tau} \\ e_i\boldsymbol{u} - \boldsymbol{\tau}\cdot\boldsymbol{u} - k\nabla T \end{vmatrix}, \qquad \boldsymbol{Q} = \begin{vmatrix} 0 \\ \boldsymbol{J}\times\boldsymbol{B} \\ \boldsymbol{E}\cdot\boldsymbol{J} \end{vmatrix}$$

The physical model of the electrodynamics has been obtained assuming the condition $Re_m \ll 1$. Under this assumption, some useful approximations can be applied.[2,3] Most notably, when an externally generated magnetic flux density $\boldsymbol{B}_0$ is applied to the plasma flow (i.e., a magnetic flux density produced by electric current), the magnetic flux density $\boldsymbol{B}_j$ due to the current density in the plasma can be neglected. Thus, the total magnetic flux density $\boldsymbol{B}$ may be considered equal to the externally applied field $\boldsymbol{B}_0$. Furthermore, assuming that the applied magnetic flux density does not vary in time or varies slowly, one can neglect the time derivative term in the Faraday–Lenz law:

$$\nabla \times \boldsymbol{E} = 0 \tag{3}$$

Another convenient approximation can be utilized, assuming that the characteristic time for the macroscopic variations is much greater than the inverse of the plasma frequency:

$$t_c \gg \omega_p^{-1} \tag{4}$$

When Eq. (4) holds, the displacement current density, given by the time derivative of the displacement field $\boldsymbol{D}$, may be neglected compared to the conduction current density.[3] The Ampere–Maxwell law can then be rewritten as follows:

$$\nabla \times \boldsymbol{H} = \boldsymbol{J} \tag{5}$$

According to Eq. (3), the irrotational electric field $\boldsymbol{E}$ may be expressed as the gradient of a scalar potential φ:

$$\boldsymbol{E} = -\nabla\varphi \tag{6}$$

Applying the divergence operator to Eq. (5), the following equation can be written as well:

$$\nabla \cdot \boldsymbol{J} = 0 \tag{7}$$

The electrodynamic model is completed by the generalized Ohm law, which is here reported by neglecting the ion Hall parameter and the electron pressure gradient:

$$\boldsymbol{J} = \sigma(\boldsymbol{E} + \boldsymbol{u}\times\boldsymbol{B}) - \beta_e[(\boldsymbol{J}\times\boldsymbol{B})/B] \tag{8}$$

where

$$\beta_e = \mu_e B \tag{9}$$

An explicit two-dimensional model has been developed for the solution of the MHD problem.[3] Referring to Fig. 1, an x–y plane is utilized as calculation domain. In the reference system fixed with the body, the gaseous medium flows with hypersonic velocity $\boldsymbol{u}$ lying on the x–y plane, while the z component of the velocity is neglected. The magnetic flux density $\boldsymbol{B}$ generating the MHD interaction lies on the x–y plane too. Thus, the electromotive force $\boldsymbol{u}\times\boldsymbol{B}$ is directed along the z axis. The current density $\boldsymbol{J}$ has a component along the z axis and a Hall component on the x–y plane.

At each time step the space discretization is performed. A cell-centered finite volume formulation, based on a Galerkin approach, has been adopted for the spatial discretization of the fluid dynamics.[4] Fluxes are evaluated by means of a centered scheme corrected by an Osher scheme.[5] Second-order accuracy is obtained, utilizing a MUSCL[6] approach, by a combination of upwind and centered discretization of the gradient. Turbulent fluxes are calculated by means of a k–ε method.

Time integration is performed utilizing an explicit scheme based on a fourth-order Runge–Kutta method. In the given two-dimensional geometry, generalized Ohm's equation (8) can be rewritten as

$$\boldsymbol{J} = \boldsymbol{\sigma}(\boldsymbol{E} + \boldsymbol{u}\times\boldsymbol{B}) \tag{10}$$

where the conductivity tensor in the considered two-dimensional geometry has the following expression:

$$\boldsymbol{\sigma} = \frac{\sigma}{1+\beta_e^2}\begin{bmatrix} 1+\beta_x^2 & \beta_x\beta_y & \beta_y \\ \beta_x\beta_y & 1+\beta_y^2 & -\beta_x \\ -\beta_y & \beta_x & 1 \end{bmatrix}$$

$$\beta_x = B_x\frac{\beta_e}{B} = \mu_e B_x, \qquad \beta_y = B_y\frac{\beta_e}{B} = \mu_e B_y$$

It is worth noting that the aforementioned assumptions lead to a steady-state electrodynamics, described by means of an elliptical partial differential equation, which can be derived from Eqs. (6), (7), and (10):

$$\nabla\cdot[\boldsymbol{\sigma}(-\nabla\varphi + \boldsymbol{u}\times\boldsymbol{B})] = 0 \tag{11}$$

This does not mean that the electrodynamic quantities do not vary in time. Electrodynamics may rather be considered to vary as a sequence of steady-state solutions driven by the evolution in time of the fluid dynamics. This is because, in the frame of the assumptions described earlier, the electrodynamics has a negligible characteristic time compared to the fluid dynamics. Electrodynamic quantities are accordingly assumed to adapt themselves instantaneously to the time variation of the flowfield. Introducing the forcing term

$$\boldsymbol{F} = \boldsymbol{\sigma}(\boldsymbol{u}\times\boldsymbol{B})$$

defined in the given two-dimensional geometry as

$$\boldsymbol{F} = \frac{\sigma}{1+\beta_e^2}(u_x B_y - u_y B_x)\begin{bmatrix} \beta_y \\ -\beta_x \\ 1 \end{bmatrix}$$

generalized Ohm's equation (11) can be conveniently rewritten as follows:

$$\boldsymbol{J} = \boldsymbol{\sigma}\boldsymbol{E} + \boldsymbol{F} \tag{12}$$

Electrodynamics is discretized by means of a finite element approach based on a variational formulation.[7] The finite element method utilized to discretize the electrodynamics is based on the following formulation of the Poynting theorem:

$$\int_S \varphi\boldsymbol{J}\cdot\boldsymbol{n}\,\mathrm{d}S = -\int_V \boldsymbol{E}\cdot\boldsymbol{J}\,\mathrm{d}V \tag{13}$$

where V and S are, respectively, the volume and the boundary surface of the calculation domain. In the two-dimensional calculation domain, a variational formulation is obtained:

$$\int_\Gamma (\partial\varphi)\boldsymbol{J}\,\mathrm{d}l - \int_\Omega \nabla(\partial\varphi)\cdot\boldsymbol{J}\,\mathrm{d}S = 0 \tag{14}$$

where Ω and Γ are the two-dimensional domain and its boundary, respectively.

The calculation domain is discretized by means of an unstructured triangular mesh. On the discretized domain an approximate scalar potential φ^* can be introduced by means of the shape functions $\{N\}$:

$$\varphi^*(x, y) = \{N\}^T\{\varphi\} \tag{15}$$

where $\{\varphi\}$ is an array containing the nodal value of the unknown electric scalar potential. An expression for the approximate electric field and current density may be written, introducing Eq. (15) in Eqs. (6) and (11):

$$\boldsymbol{E}^* = -[\nabla N]\{\varphi\} \tag{16a}$$

$$\boldsymbol{J}^* = -\boldsymbol{\sigma}[\nabla N]\{\varphi\} + \boldsymbol{F} \tag{16b}$$

Substituting Eqs. (16a) and (16b) in Eq. (14) a matrix equation is derived:

$$[K]\{\varphi\} = -\{P_J\} + \{P_F\} \tag{17}$$

The matrix $[K]$ is the conductivity matrix, defined as follows:

$$[K] = \int_\Omega [\nabla N]^T \boldsymbol{\sigma} [\nabla N]\, \mathrm{d}S \tag{18}$$

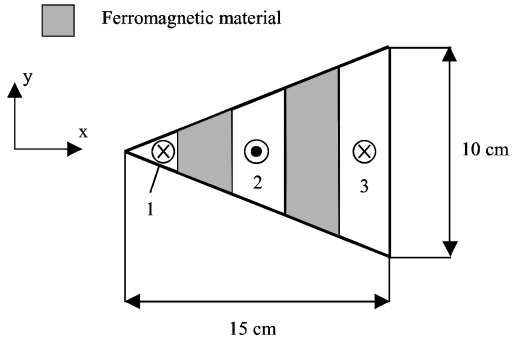

Fig. 2 Schematic of the wedge.

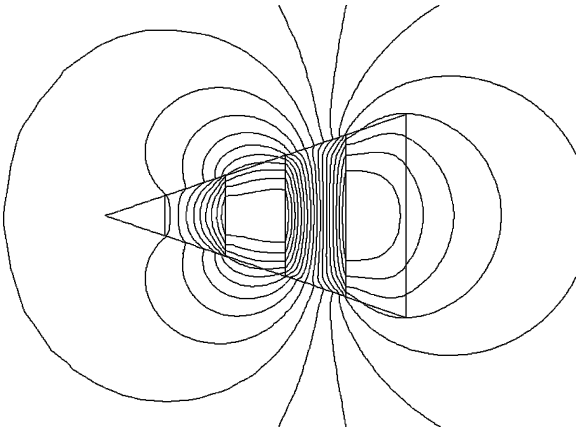

Fig. 3 Magnetic flux density around the wedge.

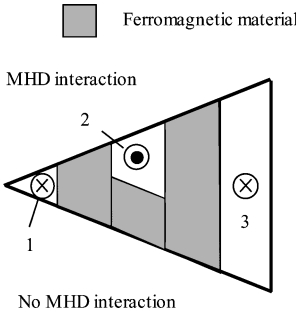

Fig. 4 Schematic of the wedge.

The array $\{P_J\}$ is the contribution of the current imposed on the boundary of the calculation domain:

$$\{P_J\} = \int_\Gamma \{N\} J_n\, \mathrm{d}l \tag{19}$$

where J_n is the current density component normal to Γ. The array $\{P_F\}$ represents the effect of the interaction between the flow and the magnetic flux density:

$$\{P_F\} = \int_\Omega [\nabla N]^T \boldsymbol{F}\, \mathrm{d}S \tag{20}$$

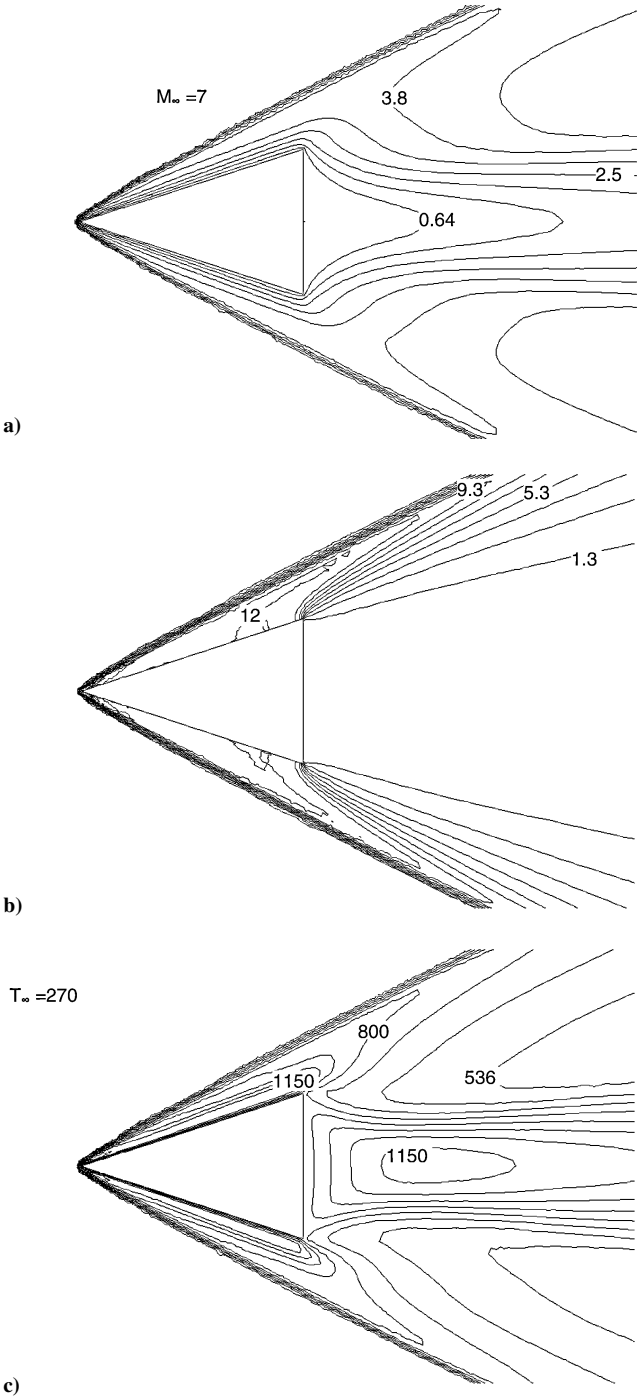

Fig. 5 Without MHD interaction: a) Mach lines, b) isobars, and c) isothermals. Values shown in the isobars plot are the ratio p/p_∞; temperature values are shown in Kelvin.

The coupling between the fluid and the electrodynamics is accomplished quite straightforwardly.[8,9] As previously stated, the time-dependent behavior of the model is governed by the fluid dynamics. At the generic nth time step, the fluid dynamic solver evaluates the source terms in the continuity equation for momentum and energy utilizing the values of $\boldsymbol{E}$ and $\boldsymbol{J}$ calculated at the previous time step. The steady-state electrodynamic model then utilizes the value of $\boldsymbol{u}$ at the nth step to compute $\boldsymbol{E}$ and $\boldsymbol{J}$. These quantities will be utilized as input for the $(n+1)$th time step of the fluid dynamic solver.

Applications

The model described has been utilized to analyze the MHD field over a wedge in the hypersonic regime. The dimensions of the considered body are shown in Fig. 2, where the position of the conductors are shown as well. The considered body includes two segments of a ferromagnetic material, which constitute a preferential path for the magnetic flux. This allows a reduction of the current needed to generate a given magnetic flux and gives some degree of control on the distribution of the magnetic flux density lines. The conductor windings are deployed so that the total current flowing in section 2 in Fig. 2 is equal to the sum of the currents flowing in sections 1 and 3. The distribution of the magnetic flux density produced by the described arrangement is shown in Fig. 3. When the current I_2 is equal to 52 kA, the magnetic flux density is about 1 T on the surface of the wedge, with a maximum of 2.29 T.

The wedge can be arranged in a differential configuration, shown in Fig. 4. In this arrangement, the magnetic flux density, being confined in the ferromagnetic core, will be almost null in the lower boundary layer of the wedge. As a consequence, the forces caused by the MHD interaction will act only on the upper side of the wedge.

To carry out the experimental activity, a wind-tunnel facility, located at the Centrospazio Laboratories, Pisa, Italy, capable of producing a hypersonic flow up to Mach 7, is utilized. Thus, the MHD regime around the wedge subject to a Mach 7 airflow is analyzed. A freestream flow with 76 Pa pressure and 9.8 10^{-4} kg $\cdot$ m^{-3} density is considered in order to simulate the condition of a vehicle at a 50-km altitude. Under these conditions, the upstream flow velocity is 2310 m $\cdot$ s^{-1}.

The calculation of the flow condition around the wedge was performed on a 26,000-node unstructured triangular mesh. The calculated Mach line, isobar, and isothermal distributions when no MHD interaction is present are shown in Figs. 5a, 5b, and 5c, respectively.

To estimate the conductivity and Hall parameter, a 50 T^{-1} constant electron mobility has been assumed. This value corresponds roughly to the mobility in the boundary-layer region. As a result, the electron Hall parameter depends only on the magnetic flux density distribution, accordingly to Eq. (9). Assuming an ionization degree of 10^{-3}, the higher value of the conductivity is 360 S m^{-1}, in the denser region near the wedge walls.

A first calculation has been performed to evaluate the effects of the MHD interaction when neglecting the hall current. The calculation results are shown in Figs. 6a, 6b, and 6c, where Mach lines, isobars,

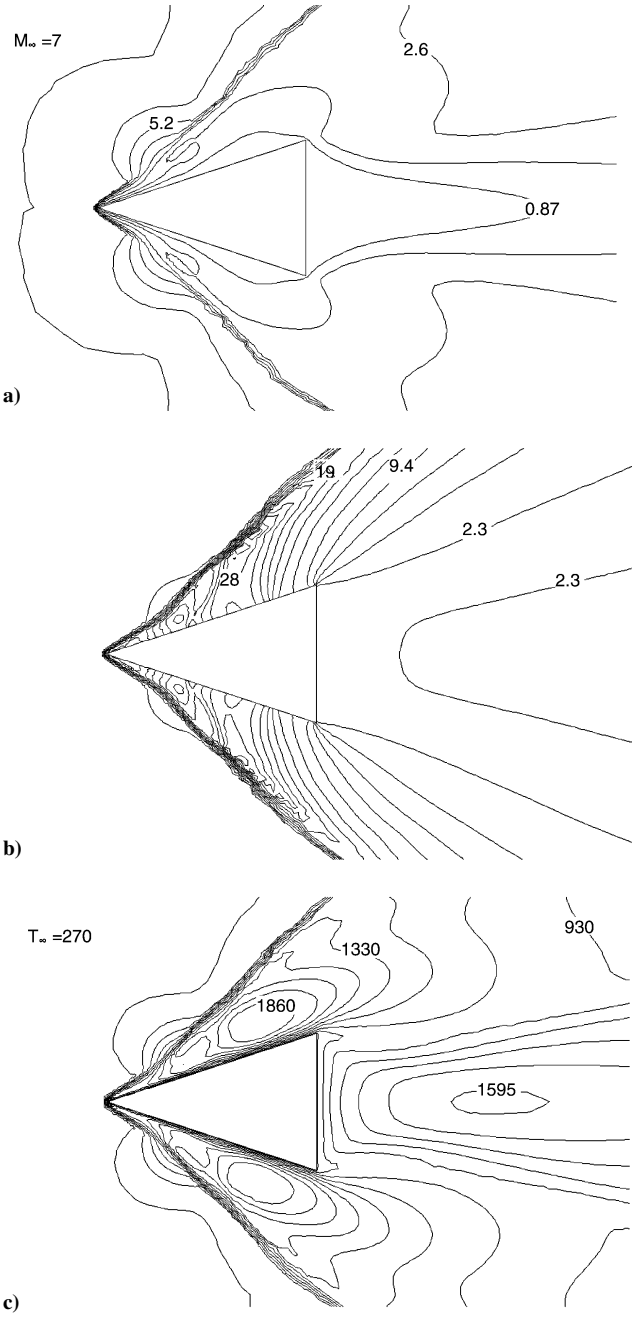

Fig. 6 With MHD interaction neglecting the Hall parameter: a) Mach lines, b) isobars, and c) isothermals. Values shown in the isobar plot are the ratio p/p_∞; temperature values are shown in Kelvin.

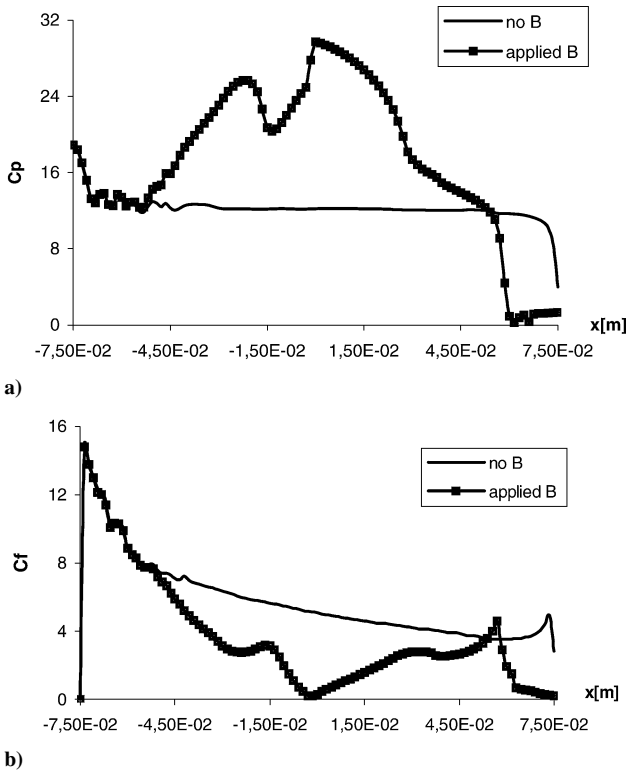

Fig. 7 Comparison with and without the applied magnetic flux density when the Hall parameter is neglected: a) pressure coefficient and b) friction coefficient.

and isothermals are plotted, respectively. As can be easily noted, the evaluated MHD interactions strongly affect the flow around the wedge.

The pressure coefficient c_p, defined as the ratio between the gas pressure and the free-flow pressure p_{in}, is along the body wall in the leading-edge region (reported in Fig. 7a) and is compared with the pressure coefficient with no applied magnetic flux density. The leading-edge vertex is the origin of the x axis. The reduction of the airspeed caused by the specific force $\boldsymbol{J} \times \boldsymbol{B}$ generates a pressure rise along the wedge sides. The integrals of the forces along the direction normal to the wedge sides due to the wall pressure increase by more than 100%. In Fig. 7b, the friction coefficient c_f, defined as the ratio between the viscous stress on the wedge wall τ_w and the free-flow pressure, is plotted along the body wall with and without the applied magnetic flux density. The MHD interaction causes a decrease of the viscous stresses as a consequence of the decreased flow velocity gradient. The integrals of the drag forces along the wedge sides are decreased by 36% due to the MHD interaction.

The analysis performed next includes the effects of the Hall parameter. Two electrical configurations have been studied. In the first configuration, the current density normal to the wedge walls is set to zero (insulating walls configuration). In the second configuration, the wedge walls are set to the same electric potential (shorted wall configuration). In Figs. 8a, 8b, and 8c, Mach lines, isobars, and isothermals are plotted, respectively, in the case of insulating wedge walls. In this case, MHD effects are drastically reduced. In the pressure and friction coefficient plot, reported in Figs. 9a and 9b, it can be noted that the pressure along the wedge side weakly increases when the magnetic flux density is applied, whereas the friction coefficient remain largely unaffected. In this case, the variation of the integral values of normal pressure and drag force are +2 and +6%, respectively. The same evidence is obtained for the shorted wedge walls. In Figs. 10a and 10b, the pressure and the friction coefficient are reported. The integrated pressure along the wedge wall increases by 4%, while the variation of the integral value of the drag force is less than +1%.

The forces per unit width due to pressure and friction stresses $\boldsymbol{f}_p$ and $\boldsymbol{f}_f$ can be obtained as follows:

$$\boldsymbol{f}_p = -\left(\int P \, \mathrm{d}l\right)\boldsymbol{n} = -\left(P_{\text{in}} \int c_P \, \mathrm{d}l\right)\boldsymbol{n} \tag{21}$$

$$\boldsymbol{f}_f = \left(\int \tau_w \, \mathrm{d}l\right)t = \left(P_{\text{in}} \int c_f \, \mathrm{d}l\right)t \tag{22}$$

The integrals in Eqs. (21) and (22) are carried on the walls of the wedge. Utilizing the obtained results, the forces modules f'_p and f'_f acting on each wedge side are about 140 and 10 $\mathrm{N \cdot m^{-1}}$. The calculations show that, for insulating walls configuration, the expected variation of the forces modules $\Delta f'_p$ and $\Delta f'_f$ due to the

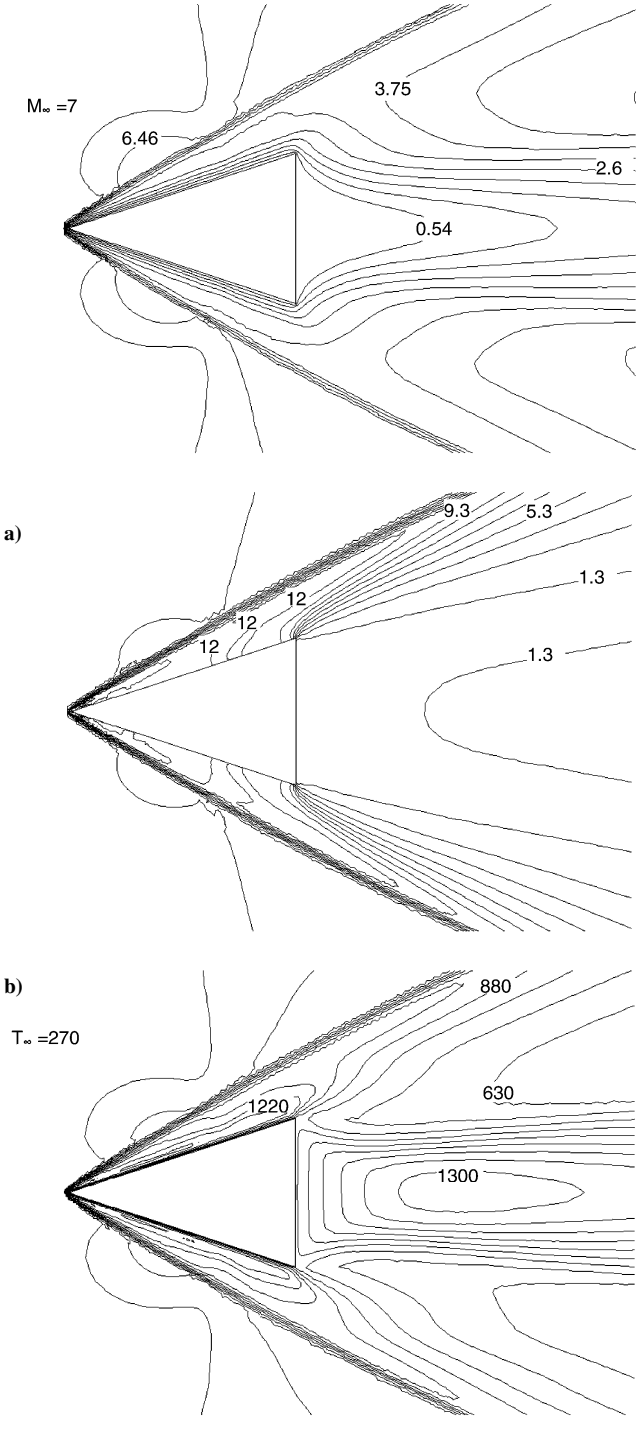

Fig. 8 With MHD interaction (insulating wedge walls configuration): a) Mach lines, b) isobars, and c) isothermals. Values shown in the isobar plot are the ratio p/p_∞; temperature values are shown in Kelvin.

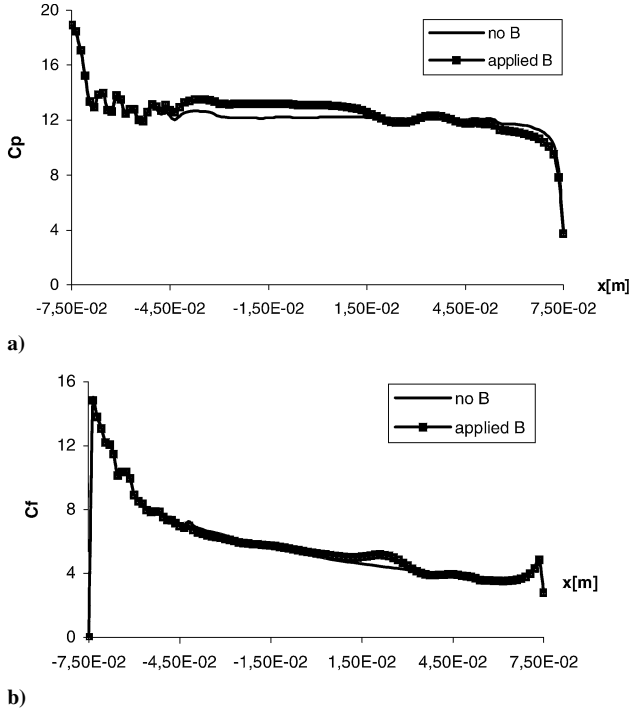

Fig. 9 Comparison with and without the applied magnetic flux density in the insulating wedge configuration: a) pressure coefficient and b) friction coefficient.

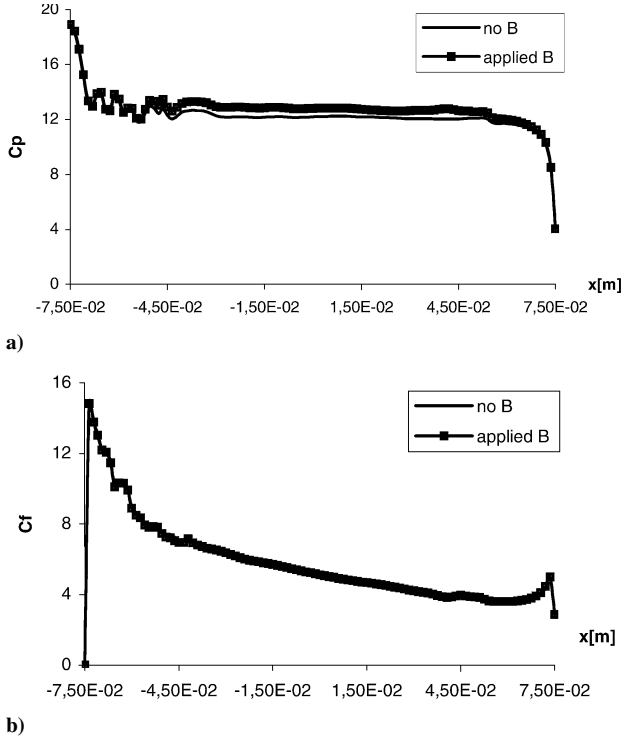

Fig. 10 Comparison with and without the applied magnetic flux density in the shorted wall configuration: a) pressure coefficient and b) friction coefficient.

MHD interaction are 3.11 and 0.62 $\mathrm{N}\cdot\mathrm{m}^{-1}$. For the shorted walls configuration, $\Delta f'_p = 5.56\ \mathrm{N}\cdot\mathrm{m}^{-1}$ and $\Delta f'_f = 0.089\ \mathrm{N}\cdot\mathrm{m}^{-1}$.

The differential configuration, shown in Fig. 3, may be conveniently utilized to estimate $\Delta f'_p$. In this condition, neglecting the effect of the MHD interaction on the lower edge side, the total force per unit width f_y acting on the wedge in the y direction is

$$f_y = -\Delta f'_p \cos(\alpha/2) + \Delta f'_f \sin(\alpha/2) \approx -\Delta f'_p \cos(\alpha/2)$$

where α is the wedge angle. By measuring f_y, $\Delta f'_p$ can be evaluated. The measurement of the variation of the total force in the x direction for the wedge in the configuration shown in Fig. 1 can then be utilized to evaluate $\Delta f'_f$ by means of the following expression:

$$\Delta f_x = \Delta f'_p \sin(\alpha/2) + \Delta f'_f \cos(\alpha/2)$$

Conclusions

In this paper, a model for the analysis of MHD interaction in hypersonic regimes with low magnetic Reynolds numbers is presented. The model consists of the Navier–Stokes equations, Maxwell equations, and generalized Ohm's law. Fluid dynamics is solved utilizing a MUSCL approach. Electrodynamics is discretized by means of a finite element technique. An explicit scheme, based on a fourth-order Runge–Kutta method, is utilized for the time integration process. The model has been applied for the analysis of the MHD interaction in the boundary layer of a hypersonic wedge. Calculations show that MHD interaction can be significantly weakened by the Hall current phenomenon.

Acknowledgment

This work was performed in the frame of the "MHD Interaction in Hypersonic Flows" research project funded by the Italian Space Agency.

References

[1]Bityurin, V. A., Botcharov, A. N., Potebnya, V. G., and Lineberry, J. T., "MHD Effects in Hypersonic Flows Around Blunt Body," *2nd Workshop on Magneto Plasma Aerodynamics in Aerospace Applications*, Inst. for High Temperature of Russian Academy of Sciences, Moscow, 2000, pp. 46–55.

[2]Rosa, J. R., *Magnetohydrodynamics Energy Conversion*, McGraw–Hill, New York, 1968.

[3]Mitchner, M., and Kruger, C. H., *Partially Ionized Gases*, Wiley-Interscience, New York, 1973.

[4]Fezoui, L., and Stoufflet, B., "A Class of Implicit Schemes for Euler Simulations on Unstructured Meshes," *Journal of Computational Physics*, Vol. 84, 1989, pp. 174–206.

[5]Oesher, S., and Solomon, F., "Upwind Difference Schemes for the Hyperbolic Systems of Conservation Laws," *Mathematics of Computation*, Vol. 38, 1982, pp. 339–374.

[6]Laney, C. B., *Computational Gasdynamics*, Cambridge Univ. Press, Cambridge, England, U.K., 1998, Chap. 23.

[7]Borghi, C. A., Cristofolini, A., and Minak, G., "Numerical Methods for the Solution of the Electrodynamic Problem in Magnetohydrodynamic Flows," *IEEE Transactions on Magnetics*, Vol. 32, No. 3, 1996, pp. 1010–1013.

[8]Borghi, C. A., Cristofolini, A., and Ribani, P. L., "Analysys of Magneto-Plasma Dynamic Transients in a Combustion Gas Magnetohydrodynamic Generator," *Physics of Plasma*, Vol. 4, No. 8, 1997, pp. 3082–3090.

[9]Borghi, C. A., and Cristofolini, A., "A Hybrid Implicit Numerical Method for the Analysis of the Magneto-Plasmadynamics in a Gas Discharge," *IEEE Transactions on Magnetics*, Vol. 37, No. 5, 2001, pp. 3401–3404.

A. Ketsdever
Associate Editor